Journal of Magnetic Resonance **155,** 72–82 (2002)
doi:10.1006/jmre.2001.2498, available online at http://www.idealibrary.com on IDEAL®

Direct Conversion of EPR Dipolar Time Evolution Data to Distance Distributions

Gunnar Jeschke, Achim Koch, Ulrich Jonas, and Adelheid Godt

Max-Planck-Institut für Polymerforschung, Postfach 3148, 55028 Mainz, Germany

Received August 20, 2001; revised November 26, 2001; published online February 8, 2002

Shallow electron spin echo envelope modulations due to dipole–dipole couplings between electron spins provide information on the radial distribution function of the spins in disordered systems while angular correlations between spin pairs are negligible. Under these conditions and in the absence of orientational selection, the dipolar time evolution data can be quantitatively simulated for arbitrary radial distribution functions by shell factorization, i.e., by performing the orientational average separately for thin spherical shells and multiplying the signals of all the shells. For distances below 5 nm, a linear superposition of the signals of the shells is sufficient. The dipolar time evolution data can be separated into this linear contribution and a nonlinear background. The linear contribution can then be converted directly to a radial distribution function. For a series of shape-persistent and flexible biradicals with end-to-end distances between 2 and 5 nm, shell factorization and direct conversion of the data are in good agreement with each other and with force-field computations of the end-to-end distances. The neglect of orientation selection does not cause significant distortions of the determined distance distributions.

Key Words: **pulse EPR; solid state; distance measurements; nitroxide; radial distribution function.**

INTRODUCTION

Electron paramagnetic resonance (EPR) spectroscopy is one of only a few methods that can precisely measure distances in the range between 1 and 10 nm in disordered systems (*1*). For complex systems, EPR spectroscopy may be the only practical method, since techniques such as small-angle x-ray scattering (*2*) and small-angle neutron scattering (*3*) suffer from insufficient contrast, and fluorescence resonance energy transfer (*4*) depends on pairs of different fluorescence labels. Attaching two different labels may be synthetically more demanding than attaching two like paramagnetic labels. Furthermore, the larger fluorescence labels may cause larger structure perturbations in the system. As the characterization of structures in the distance range between 1 and 10 nm is crucial for both the development of nanomaterials and the understanding of the function of biological systems, further development of methodology for distance measurements between electron spins is of great interest.

While continuous-wave EPR is well suited to the distance range between 1 and 2 nm (*1*), larger distances have to be measured by modern pulse techniques (*5*) that separate the dipole–dipole interaction of the electron spins from all the other interactions (*6–17*). Using one of these techniques and suitably functionalized nitroxide spin probes, we have recently succeeded in measuring spin–spin distance distributions between 1.8 and 8 nm (*18*). We could thus study how the size of and the distances between ionic clusters in block copolymer-based ionomers depend on polymer chain length (*19*). In these investigations we could fit simple models for the distance distribution to the experimental dipolar time evolution data. Such analysis of data for disordered systems in terms of simple models was also performed by other authors (*20–22*). For general applications it would be much more favorable to directly convert such data to a distance distribution without assuming any explicit model. Encouraging early attempts to introduce such a method (*8, 23, 24*) have not been followed up for a long time and did not find applications despite a recent surge in such measurements (*1*). In the present work, we discuss which assumptions have to be made to convert dipolar evolution data to a radial distribution function $G(r)$. We then present the shell factorization model for the simulation of dipolar time evolution data for arbitrary distance distributions and derive the mathematics for a simple and fast direct conversion procedure. Finally, this procedure is tested on experimental data for both shape-persistent and flexible nitroxide biradicals with end-to-end distances between 2 and 5 nm.

THEORY

Relation between Dipolar Time Evolution and the Radial Distribution Function

Consider experiments such as three-pulse DEER (*6, 9*), four-pulse DEER (*10, 11*), and double-quantum EPR (*13–15*) for which the dipolar time evolution signal for a single pair (i, k) of localized electron spins with distance r_{ik} is given by

$$V(t) = V_0[1 - \lambda_{ik}(1 - \cos(\omega_{ik}t))], \qquad [1]$$

where the modulation depth λ_{ik} quantifies the fraction of the echo signal that is due to excited spin pairs (i, k) and

$$\omega_{ik} = \omega_{\mathrm{dd}}^{(ik)}(3\cos^2\theta_{ik} - 1) \qquad [2]$$

1090-7807/02 $35.00

with

$$\omega_{\mathrm{dd}}^{(ik)} = \frac{\mu_0}{4\pi\hbar}\frac{g_i g_k \mu_{\mathrm{B}}^2}{r_{ik}^3} \qquad [3]$$

is the dipolar evolution frequency. Without losing generality we may treat spin i as an observer spin (A spin) and spin k as a pumped spin (B spin). The parameters g_i and g_k are the electron g values of the two spins, and θ_{ik} is the angle between the static field vector $\boldsymbol{B}_0$ and the vector connecting the loci of the two spins. Henceforth we assume $g_i = g_k = g$ for all i, k. In a sample containing multispin systems, the signal for any A spin is thus given by

$$V_i(t) = V_{0,i}\prod_{k\neq i}[1 - \lambda_{ik}(1 - \cos(\omega_{ik}t))] \qquad [4]$$

and the total signal is the sum of the signals for all A spins $\sum_i V_i(t)$. The macroscopic sample can be described as an ensemble of a very large number of such multispin systems, which are in turn configurations of n spins that are completely characterized by $n-1$ pairs of distances and angles (r_{ik}, θ_{ik}). For a given experiment, we only need to consider B spins with $r_{\min} \leq r_{ik} \leq r_{\max}(t_{\max})$, where $r_{\min}$ is determined by the bandwidth of the pulses, as discussed below, and $r_{\max}$ is a distance for which the dipolar time evolution does not lead to a perceptible echo decay within the observation time of the experiment. In the following we assume macroscopic disorder, i.e., the orientation of the molecular frame is not correlated to the orientation of $\boldsymbol{B}_0$.

For a discussion of structure determination of such macroscopically disordered systems from $\sum_i V_i(t)$ it is useful to examine first the two limiting cases of complete local order and complete disorder. For complete order at the length scale $r_{\min} \leq r \leq r_{\max}$, as is encountered in a powder of ideal crystallites, all A spins see the same configuration of $n-1$ B spins. A Cartesian local frame is defined by the A spin and the first two B spins. The relevant parameters are the distances r_{i1} and r_{i2} between the A spin the two B spins and the the angle between the two A–B spin–spin vectors. Each additional B spin adds three parameters, the distance r_{ik} and the polar angles θ_k and ϕ_k in the local frame. Hence the total number of parameters characterizing such a structure with complete local order is $3(n-2)$. Due to the general symmetry properties of the spin Hamiltonian and due to resolution limitations it may be impossible to determine all these parameters from $V(t)$. On the other hand it may be possible to correlate the local frame of the spin distribution to the molecular frame determined by the g or hyperfine tensor by making use of orientation selection (*16, 17*). In the following, we neglect orientation selection effects. Their influence on the apparent distance distribution will be considered in the experimental section.

Complete disorder corresponds to a homogeneous distribution of spins with no correlation between the θ_{ik} and a distance distribution function $p(r_{ik}) \propto 4\pi r^2$. It has been demonstrated earlier (*25, 26*) that in this case the system is fully characterized by the concentration C of spins. The dipolar time evolution is a monoexponential decay $V(t) = V_0\exp(-t/T_{\mathrm{hom}})$ with time constant

$$T_{\mathrm{hom}} = \frac{9\sqrt{3}\hbar}{2\pi g^2\mu_{\mathrm{B}}^2\mu_0\lambda C}, \qquad [5]$$

where the modulation depth parameter λ is the fraction of excited B spins.

For systems with intermediate order, the structure is characterized by the distance distribution function $p(r) = 4\pi r^2 G(r)$, where $G(r)$ is the radial distribution function, and by correlations between the θ_{ik}. By expanding the product on the right-hand side of Eq. [4] and computing $\sum_i V_i(t)$ we find that the effect of the distance distribution on the echo signal is linear in λ, while the effect of correlations between m angles θ_{ik} scales with λ^m. For $\lambda \ll 1$, which is usually fulfilled in DEER experiments on nitroxide spin probes, the dipolar time evolution is thus dominated by effects of the radial distribution function $G(r)$, even if significant correlations between the θ_{ik} exist.

Validity of the Linear Approximation and Shell Factorization Model

The direct use of Eq. [4] for numerical computations of dipolar time evolution data from a given model for the system is not feasible. As the most simple approximation we can expand the product on the right-hand side of this equation and consider only the constant term and the terms linear in the λ_{ik}. All effects of angular correlations are thus neglected. If we perform the ensemble average over the macroscopically disordered sample and neglect orientation selection, we can express the result as

$$V_{\mathrm{lin}}(t) = 1 - \int_{r_{\min}}^{r_{\max}} 4\pi r^2\lambda G(r)\left(1 - \int_0^{\pi/2}\cos\left((3\cos^2\theta - 1) \times \frac{g^2\mu_{\mathrm{B}}^2\mu_0}{4\pi\hbar}\frac{1}{r_i^3}t\right)\right)\sin\theta\, d\theta\, dr. \qquad [6]$$

Unfortunately, this approximation does not exhibit the proper asymptotic behavior for $r_{\max} \to \infty$ and does not reproduce the exponential decay with the time constant given in Eq. [5] for a homogeneous distribution of spins. The reason for this failure becomes obvious by considering the frequency dependence of the modulation depth. For large distances the dipolar modulation frequency asymptotically approaches zero, while $p(r) \propto r^2$. As a consequence, the concept of a finite modulation depth becomes obsolete at zero frequency. In other words, at sufficiently long distances the problem can no longer be treated in terms of isolated spin pairs. The linear approximation in Eq. [6] can thus only be used up to a certain distance r_{lin}.

In previous work, this problem was usually fixed by factorization of the signal into one part corresponding to isolated spin pairs with a well-defined distance (intrapair contribution) and a part corresponding to interactions between spins in different pairs (interpair contribution). To compute the interpair contribution, a homogeneous distribution of the pairs in space was assumed (*6, 9*). This contribution, which extends to $r > r_{\mathrm{lin}}$, could thus be discribed by Eq. [5]. However, the distance distribution in many systems of interest cannot be approximated by such a simple model. To perform simulations for arbitrary distance distributions, nonlinearity at long distances due to multispin contributions must be accounted for in a more general way.

In numerical computations this problem can be solved by substituting the integral over the pair correlation function by a product of a finite number of spherical shells with radii $r_{\mathrm{min}} \leq r_k \leq r_{\mathrm{max}}$ and uniform thickness Δr. By choosing Δr so that

$$4\pi r_k^2 \Delta r \lambda G(r_k) \ll 1, \qquad [7]$$

for all k, the linear approximation is valid within each shell. Such a choice is usually possible for disordered systems. We can thus perform the integration over θ (powder average) for each shell separately

$$V_k(t) = \int_0^{\pi/2} \cos\left[(3\cos^2\theta - 1)\omega_{\mathrm{dd}}(r_k)\, t\right] \sin\theta \, d\theta, \qquad [8]$$

and compute the signal as the product of the signals of all the shells

$$V(t) = \prod_k [1 - 4\pi r^2 \lambda \Delta r G(r_k)(1 - V_k(t))]. \qquad [9]$$

This *shell factorization model* exhibits the proper asymptotic behavior for $r \to \infty$, as V_k approaches $V_\infty(t) \equiv 1$ for $\omega \to 0$. To compute the dipolar time evolution signal for $t_{\mathrm{max}} \leq 8\ \mu$s we use $r_{\mathrm{min}} = 1.5$ nm, $r_{\mathrm{max}} = 40$ nm, and $\Delta r = 0.02$ nm. For typical concentrations $c = C/N_A < 5$ mmol L^{-1}, such numerical simulations for a homogeneous distribution of radicals ($G(r) \equiv C$) are in nice agreement with Eq. [5]. Figure 1 shows a numerical simulation by the shell factorization model with $\lambda c = 1$ mmol L^{-1} and $g = g_{\mathrm{e}}$ and its difference from a simulation based on Eq. [5]. The difference at early times is due to the cutoff toward short distances ($r < r_{\mathrm{min}}$) and is also expected in experimental data (for a discussion, see also Ref. *27*). In contrast, the cutoff toward longer distances ($r > r_{\mathrm{max}}$) does not lead to any significant difference, as was also checked by using larger r_{max}. Thus, for a given maximum observation time t_{max}, spins at larger distances than the appropriate r_{max} do not significantly contribute to the dipolar time evolution signal, as was already discussed qualitatively in Ref. (*6*). For a homogeneous distribution, the experiments thus measure *local* concentrations on a nanoscopic length scale.

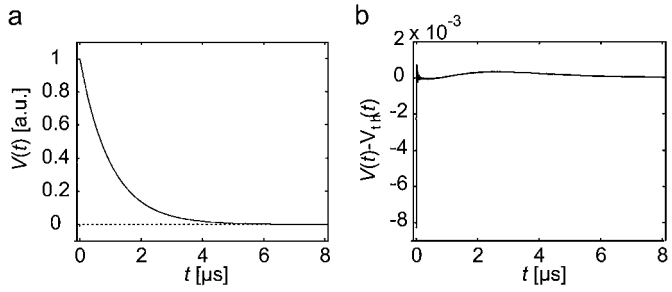

FIG. 1. Simulation of the dipolar time evolution signal $V(t)$ for a homogeneous distribution of radicals with $g = g_{\mathrm{e}}$ and $\lambda c = 1$ mmol L^{-1} by the shell factorization model ($r_{\mathrm{min}} = 1.5$ nm, $r_{\mathrm{max}} = 40$ nm, $\Delta r = 0.02$ nm). (a) Simulated signal (solid line) and difference between the simulated signal and the exponentially decaying signal with time constant $T_{\mathrm{hom}} = 1.0027\ \mu$s (Eq. [5]) computed from a closed analytical expression (dashed line). (b) Difference between numerical and analytical simulation magnified by a factor of 100.

By fitting an exponential decay to the data from the numerical simulation we obtain $T_{\mathrm{hom}} = 1.0041\ \mu$s in good agreement with the theoretical value of $1.0027\ \mu$s. Except for the discretization of r, the shell factorization model is also in full agreement with the analytical formula for an ensemble of isolated spin pairs with a common distance r. The approximations in this model thus hold for both limiting cases of a distance distribution, the homogeneous distribution and a distribution consisting of a single δ peak. Any distance distribution is an intermediate case between these two limits; therefore, the approximations should also apply.

The shell factorization model can thus be used to simulate the corresponding dipolar time evolution data for arbitrary distance distributions, as long as Δr can be made small enough so that Eq. [7] applies over the whole interval $(r_{\mathrm{min}}, r_{\mathrm{max}})$. Such computations are much less time consuming than Monte Carlo simulations which treat the multispin contribution explicitly (*20*), which is particularly important for nonlinear fitting of experimental data to model distributions with several parameters. Furthermore, by comparing such simulations with computations according to the simple linear approximation (Eq. [6]), we can estimate r_{lin}. Depending on the modulation depth λ and the required precision in the simulation (signal-to-noise ratio, required precision for the estimated $G(r)$), we find $r_{\mathrm{lin}} \approx 4 \cdots 6$ nm.

As was pointed out by a referee, we may expand the product in Eq. [9]; let $\Delta r \to 0$, and replace the series by an exponential, resulting in

$$V(t) = \exp[V_{\mathrm{lin}}(t) - 1], \qquad [10]$$

where $V_{\mathrm{lin}}(t)$ is given by Eq. [6]. Note that plots of $\ln V(t)$ have been used extensively in earlier work (*9, 22*). If the signal-to-noise ratio is sufficient, the direct transformation of the linear contribution described in a later section should thus also be applicable to $\ln V(t) + 1$.

Separation of Linear and Nonlinear Contributions

A "model-free" conversion of dipolar time evolution data to a radial distribution function is expected to be much simpler within the linear approximation than for data containing nonlinear contributions. While the shell factorization model is generally applicable, we here consider direct conversion only for the linear part of the distance distribution in cases where it is well separated from the nonlinear part. Formally, we can write the signal as the product of the nonlinear and linear contributions

$$V(t) = V_{\text{nlin}}\left[1 - \lambda\left(1 - \int_{r_{\min}}^{r_{\text{lin}}} 4\pi r^2 G(r) V_r(t)\, dr\right)\right], \quad [11]$$

where $V_r(t)$ is the dipolar evolution function for a spin pair with distance r. To find a good approximation of V_{nlin}, we may note that spin pairs at short distances contribute components at large frequencies over the whole time range, but components at low frequencies only at short times (Fig. 2). Therefore, we can find a time t_1 at which the low-frequency parts of pairs at $r < r_{\text{lin}}$ have completely decayed and the linear contribution is a sum of high-frequency oscillations (*6*). Spin pairs at long distances do not contribute high frequencies, but their contributions at low frequencies is observed at all times. We can thus fit the nonlinear background for $t > t_1$ by a low-order polynomial

$$B(t) = \sum_{i=1}^{q} a_i t^i \approx V_{\text{nlin}}(1 - \lambda) \quad [12]$$

with order q and may reasonably expect that an extrapolation of this fit to the range $0 \le t \le t_{\text{lin}}$ provides a good approximation of the nonlinear contributions at early times. Such a fit with a low-order polynomial is superior to a fit by an exponential, as it can compensate for peaks in the distance distribution at $r > r_{\text{lin}}$, as long as such peaks are well separated from the peaks at $r < r_{\text{lin}}$. The linear contribution is then given by

$$V_{\text{lin}}(t) = \frac{V(t) - B(t)}{B(t)} \approx \frac{\lambda}{1 - \lambda} \int_{r_{\min}}^{r_{\text{lin}}} 4\pi r^2 G(r) V_r(t)\, dr. \quad [13]$$

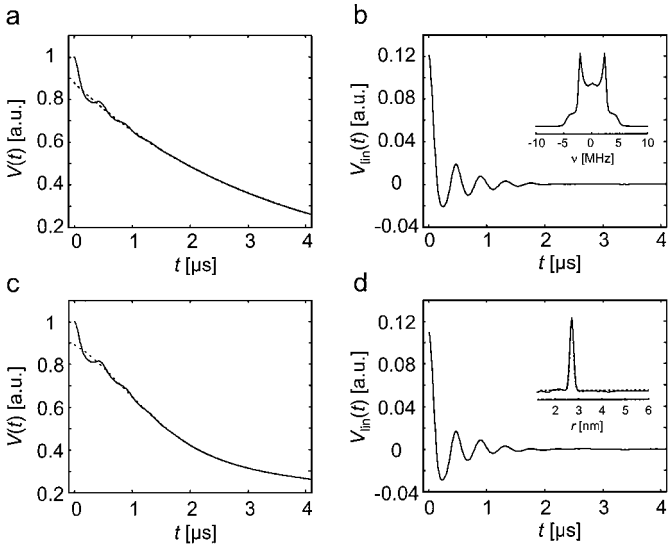

FIG. 2. Removal of nonlinear contributions by subtraction of a low-order polynomial. (a) Simulation of $V(t)$ by the shell factorization model with a distance distribution with a homogeneous background with $\lambda c = 0.3$ mmol L^{-1} and a Gaussian peak at $r = 2.8$ nm with a width of 0.1 nm. The dashed line is a fit with a third-order polynomial for $t \ge 0.5$ μs. (b) The difference of the simulated signal in (a) and the fitted cubic baseline corresponds approximately to the contribution of only the Gaussian peak. The inset shows the dipolar spectrum obtained by a Fourier transformation of the difference signal. (c) Simulation of $V(t)$ by the shell factorization model with a distance distribution with a homogeneous background with $\lambda c = 0.15$ mmol L^{-1} and two Gaussian peaks at $r_1 = 2.8$ nm with a width of 0.1 nm and at $r_2 = 7$ nm with a width of 0.25 nm and 3.9 times larger integral intensity. The dashed line is a fit with a fifth-order polynomial for $t \ge 0.5$ μs. (d) The difference of the simulated signal in (c) and the fitted fifth-order polynomial corresponds approximately to the contribution of only the Gaussian peak at 2.8 nm (linear contribution). The inset shows the theoretical distance distribution corresponding to only the peak at 2.8 nm (dashed line) together with the result of a direct transformation of the linear contribution to distance domain (solid line).

This elimination of the nonlinear contribution is demonstrated in Figs. 2a and 2b for a simulated signal corresponding to a distance distribution with one Gaussian peak at 2.8 nm with a variance of 0.1 nm and a homogeneous background with $\lambda c = 0.3$ mmol L^{-1}. With $t_1 = 0.5$ μs a third-order polynomial ($q = 3$) provides a good fit of the background (Fig. 2a), and the subtraction of the polynomial and subsequent division by the polynomial yields the separated linear contribution to the time-domain signal, which corresponds to only the Gaussian peak (Fig. 2b). The inset in Fig. 2b shows that a Fourier transform of this separated linear contribution is in satisfying agreement with the expected Pake pattern. The procedure still works reasonably well if the distance distribution features a peak at longer distances. For a homogeneous background with $\lambda c = 0.15$ mmol L^{-1} and an additional Gaussian peak at 7 nm with a variance of 0.25 nm and an integral intensity that is 3.9 times larger than that for the peak at 2.8 nm, the nonlinear contribution due to both the homogeneous background and the peak at 7 nm can be fit by a fifth-order polynomial, again with $t_1 = 0.5$ μs (Fig. 2c). The extracted linear contribution (Fig. 2d) is in reasonable agreement with the one for a purely homogeneous background (Fig. 2b).

Assuming an exact separation of linear and nonlinear parts, the discretized mathematical model for the linear contribution is thus

$$V_{\text{lin}}(t) = \sum_{k=1}^{K} \lambda' G(r_k) V_k(t), \quad [14]$$

where k runs from 1 to k_{lin} with $r_1 = r_{\min}$ and $r_K = r_{\text{lin}}$ and $\lambda' = \lambda/(1 - \lambda)$. Deviations due to the limited precision of the

separation are mainly expected for distances close to r_{lin}. In the following we omit the prime in λ'.

Discrete Integral Transformation dePakeing

The conversion of the dipolar evolution data to the distance distribution or radial distribution function thus boils down to an inversion of Eq. [14] with known $V_k(t)$. This turns out be an ill-posed problem. However, since the dipolar frequency ω_{dd} is a strictly monotonous function of the distance r, we can rewrite Eq. [14] as

$$V_{\mathrm{lin}}(t) = \sum_l P(\omega_l) V_l(t), \qquad [15]$$

with

$$V_l(t) = \int_0^{\pi/2} \cos\left[(3\cos^2\theta - 1)\omega_l t\right] \sin\theta \; d\theta, \qquad [16]$$

where the $P(\omega_l)$ quantify a discrete distribution of dipolar frequencies at appropriate sampling points ω_l (see below). The distance distribution can be obtained from $P(\omega_l)$ by a mapping of the ω_l to r_l using Eq. [3] and by a proper scaling that is discussed in the following section. The inversion of Eq. [15] is a so-called dePakeing problem, for which several solutions of increasing sophistication have been given in the literature (*29–33*). The general dePakeing problem is still ill posed. However, we shall show now that for our special case of a continuous distribution $P(\omega)$ with a resolution limited by the conformational freedom of the spin-carrying molecules, Eq. [15] can be converted to a reasonably well-posed problem by choosing a suitable set of ω_l. This problem can be solved by an integral transformation in analogy to the Fourier transformation that is widely used in magnetic resonance spectroscopy. The approach is close in spirit to the REDOR transformation used in solid-state NMR (*34*) but implemented in a different way.

The inversion of Eq. [15] by an integral transformation requires a kernel $K(\omega_{\mathrm{dd}}t)$ so that the orthogonality condition

$$\int_0^\infty V_l(\omega_l t) K(\omega_{\mathrm{dd}} t)\, dt = \delta(\omega_l - \omega_{\mathrm{dd}}) \qquad [17]$$

is fulfilled. Instead of deriving $K(\omega_{\mathrm{dd}}t)$ analytically, we may start from an approximative kernel

$$K(\omega_{\mathrm{dd}}t) = c(\omega_{\mathrm{dd}}) V(\omega_{\mathrm{dd}}t) f(t), \qquad [18]$$

where $f(t)$ does not depend on ω_{dd} and $c(\omega_{\mathrm{dd}})$ is a normalization constant that does not depend on t. Examples for integral transforms of this kind are the Fourier transformation with $f(t) \equiv 1$ and the Bessel transformation with $f(t) = t$ (*35*). As dipolar time evolution data are closely related to Bessel functions, we also depart from $f(t) = t$. For a discretized kernel, the normalization constants $c(\omega_m)$ are then given by

$$c_m = c(\omega_m) = 1 \Big/ \int_0^\infty V_m^2(t) t\, dt. \qquad [19]$$

Furthermore we define the cross-talk matrix $\boldsymbol{d}$ for the approximative kernel by its elements

$$d_{ml} = \frac{1}{c_m} \int_0^\infty V_l(t) V_m(t) t\, dt. \qquad [20]$$

Due to normalization the diagonal elements of the cross-talk matrix are all unity. However, the matrix is not symmteric, since in general $c_m \neq c_l$ for $m \neq l$. For an exact kernel, the orthogonality condition, Eq. [17], would hold, and all off-diagonal elements of the cross-talk matrix would be zero. Nonzero off-diagonal elements correspond to an erroneous detection of frequency component ω_m due to the presence of another frequency component ω_l. The result $\boldsymbol{P}^{(0)}$ of the discrete approximative Pake transformation

$$P_m^{(0)} = \frac{1}{c_m} \sum_i V_{\mathrm{lin}}(t_i) V_m(t_i) t_i, \qquad [21]$$

where t_i runs from 0 to $t_{\max}$, is then related to the *true* dipolar frequency distribution $\boldsymbol{P}$ by

$$\boldsymbol{d}\boldsymbol{P} = \boldsymbol{P}^{(0)}. \qquad [22]$$

By solving this set of linear equations for $\boldsymbol{P}$, the true distribution is obtained.

Such a cross-talk-corrected approximative integral transformation is in principle generally applicable for the solution of inverse linear problems. However, the quality of the approximative kernel is still crucial, as it determines if the system of linear equations, Eq. [22], corresponds to an ill-posed problem or not. This can be quantified by computing the condition number of the cross-talk matrix, which is the ratio of its largest to its smallest singular value.

The construction of a good approximative kernel involves the optimization of $f(t)$ and the choice of a suitable set of ω_m, i.e., proper discretization. For our case, it can be shown that $f(t) = t$ is a good choice, as it minimizes the cross talk between dipolar frequency zero and any other frequency. This property is crucial for practical applications, as the separation of $V(t)$ into a linear and a nonlinear contribution may leave a small erroneous constant contribution in V_{lin}. To secure this property and approximate orthogonality for neighboring frequencies ω_m

and ω_{m+1}, we have to choose

$$\omega_m = \frac{\pi}{t_{\max}}\left(m + \frac{1}{4}\right), \qquad [23]$$

where m runs from 1 to $N/2 - 2$ and N is the number of points in the discrete dipolar time evolution data. The data are thus analyzed between a minimum dipolar frequency

$$\omega_{\min} = \frac{5\pi}{4t_{\max}} \qquad [24]$$

and a maximum dipolar frequency

$$\omega_{\max} = \frac{2\pi(2N-7)}{8(N-1)\Delta t}, \qquad [25]$$

where Δt is the dwell time. For a dwell time of 8 ns and $t_{\max} = 2$ μs this corresponds to a distance scale from 1.19 to 5.50 nm, which covers the whole range of interest $r_{\min} \le r \le r_{\lim}$. The condition number for the corresponding cross-talk matrix with $\Delta t = 8$ ns and $N = 256$ is 2.99. For typical experimental conditions 1 μs $\le t_{\max} \le 8$ μs, the condition number ranges between 2.98 and 3.13. Performed in this manner, dePakeing thus does not involve the solution of an ill-posed problem.

Nevertheless, dePaked spectra are significantly noisier than the Fourier transform of the time-domain data as can be seen in Fig. 3. A time-domain data set was simulated for a dipolar frequency distribution with three Gaussian peaks and a resolution of 40 kHz and white noise with an amplitude of 0.2% of the signal maximum was added (Fig. 3a). The superposition of Pake patterns obtained by Fourier transformation of these data is shown in Fig. 3b. The noise level is already significantly enhanced in the approximative Pake transform $\boldsymbol{P}^{(0)}$ (Fig. 3c), which is entirely due to the resolution enhancement achieved here by multiplying the data with $f(t) = t$. The deviation of $\boldsymbol{P}^{(0)}$ from the original distribution (dashed line) is caused by cross talk. Accordingly, the cross-talk-corrected Pake transform $\boldsymbol{P}$ agrees nicely with the original distribution. The cross-talk correction induces only a small additional increase in the noise level, as predicted by the small condition number of the cross-talk matrix. The apparent noise suppression of the more sophisticated dePakeing methods is thus due to the smoothing inherent in them.

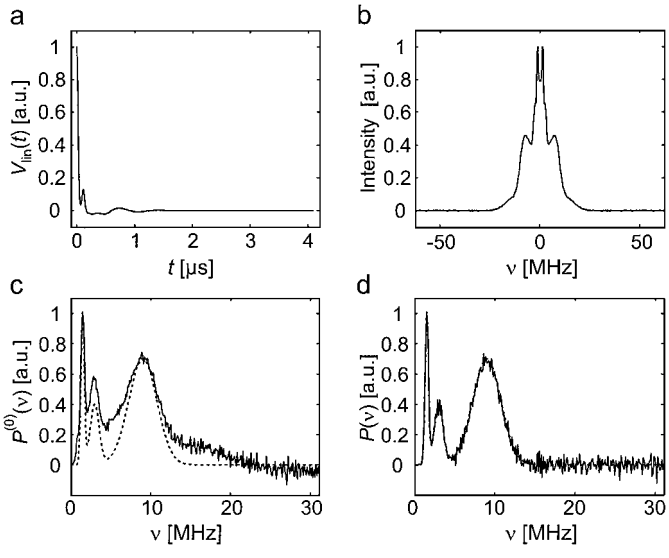

FIG. 3. Cross-talk-corrected integral transformation dePakeing. The original distribution of dipolar frequencies ω_{dd} consists of three Gaussian peaks at 1.5 MHz (variance $\sigma = 0.3$ MHz, intensity $I = 1.0$), 3 MHz ($\sigma = 0.8$ MHz, $I = 0.4$), and 9 MHz ($\sigma = 2.5$ MHz, $I = 0.7$). (a) Simulated time-domain signal with 0.2% noise added. (b) Fourier transform of the time-domain signal. (c) Approximate Pake transform $\boldsymbol{P}^{(0)}$ (solid line) and original distribution (dashed line). (d) Cross-talk-corrected Pake transform $\boldsymbol{P}$ (solid line) and original distribution (dashed line).

Distance-Domain Smoothing

Mapping the discrete distribution $\boldsymbol{P}(\omega)$ defined at equally spaced values of ω (Eq. [23]) to $G(r)$ provides a distance distribution with an ordinate spacing proportional to r^{-4}. In fact, such a spacing in the distance domain is more appropriate than an equal spacing, since for a given precision of the frequency measurement the relative error in a distance measurement scales with r^4. Furthermore, we have to consider that $\boldsymbol{P}(\omega)$ is actually mapped to $4\pi r^2 \boldsymbol{G}(r)$, so that for the discrete data we find

$$G_m = G(r(\omega_m)) = r^{-6} P(\omega_m). \qquad [26]$$

In the absence of noise, elimination of nonlinear contributions, approximate Pake transformation, cross-talk correction, and mapping yield a distance distribution which agrees almost perfectly with the theoretical distribution as can be seen, for example, in Fig. 2d.

However, the r^{-6} scaling of the amplitude increases the noise at short distances dramatically, as can be seen in Fig. 4 where the direct conversion of simulated noisy dipolar time evolution data to a distance distribution is shown. Despite the excellent signal-to-noise ratio of the original data (Figs. 4a and 4b), the distance distribution appears to be ill defined for $r < 2.2$ nm (Fig. 4c). Fortunately, this extreme scaling of the noise is caused by imposing on the data an unrealistic distance resolution at the lower end of the distance range and can thus be avoided.

Closer inspection reveals that the r^{-4} ordinate spacing of the distance distribution becomes unnecessarily fine at short distances where the precision of the distance measurement is no longer determined by the precision of the frequency measurement, but rather by the unavoidable uncertainty of the spin–spin distance due to conformational freedom and the spatial distribution of the wave function of the unpaired electron. In practice, linewidths narrower than about 0.02 nm cannot be expected in a distance distribution. It is then sensible to smooth the distance distribution based on the assumption of a realistic minimum

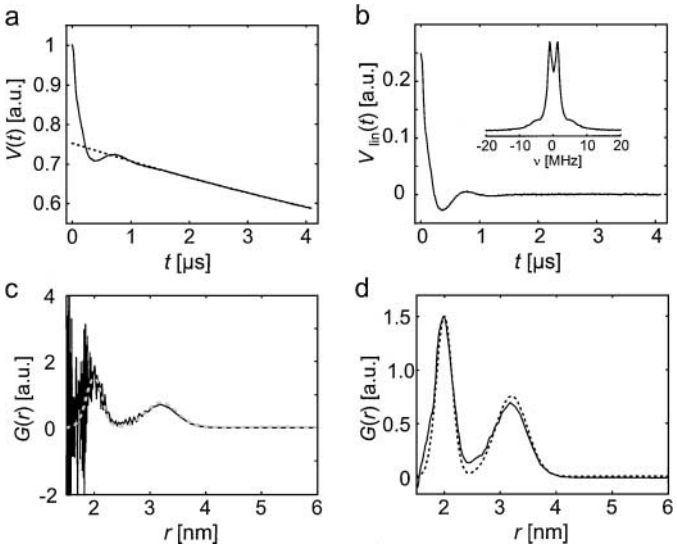

FIG. 4. Elimination of nonlinear contributions, conversion to distance domain, and distance-domain smoothing. The original distance distribution $G(r)$ consists of two Gaussian peaks at 2.0 nm (variance $\sigma = 0.2$ nm) and 3.2 nm ($\sigma = 0.4$ nm) with equal integral intensity and a homogeneous background with $\lambda c = 0.06$ mmol L^{-1}. (a) Time-domain data simulated with the shell factorization model. Noise with an rms amplitude of 0.05% of the maximum signal amplitude was added. The dashed line is a fit of the nonlinear contribution by a second-order polynomial. (b) Linear contribution to the time-domain data due to distances $r < r_{lin}$ obtained by subtraction of the polynomial. The inset shows the Fourier transform. (c) Distance distribution obtained by a cross-talk-corrected Pake transformation and mapping of $\boldsymbol{P}(\omega)$ to $4\pi r^2 \boldsymbol{G}(r)$ (solid line) and original distance distribution (gray dashed line). (d) Distance distribution obtained as in (c) but after convolution with a Gaussian function with a variance of 0.05 nm (solid line) and original distance distribution (dashed line).

peak width. Because of the r^{-4} ordinate spacing such a distance-domain smoothing has a dramatic effect on noise at short distances, as can be seen in Fig. 4d where the data of Fig. 4c are shown again, but now after convolution with a Gaussian line with a variance of 0.05 nm. The original distance distribution (dashed line) is now reproduced with satisfying precision throughout the distance range of interest. Such distance-domain smoothing is a transparent procedure in the sense that it imposes only a known, and in many cases insignificant, broadening on the true distance distribution. Furthermore, it is analogous to procedures that are well established in Fourier transform NMR and EPR spectroscopy (*5, 28*). The influence of the smoothing inherent in other kinds of data analysis, such as maximum entropy methods (*36*) or Tikhonov regularization (*37*), may be more difficult to estimate.

EXPERIMENTAL RESULTS AND DISCUSSION

Model Systems

As model systems for distance distributions with narrow peaks we used shape-persistent biradicals with end-to-end distances between 2 and 5 nm. The synthesis of these phenylene-ethynylene-based biradicals with distances between 2.8 and 5.0 nm has been described elsewhere (*38*). Their end-to-end distances were measured before by DEER and SIFTER experiments and were found to be in good agreement with the results of a force-field conformer search (*12*). The biphenyl-based biradical **3** with an end-to-end distance of approximately 2 nm was synthesized as follows:

Benzidine (155 mg, 0.84 mmol), DMAP (342 mg, 2.80 mmol), and 3-carboxy-2,2,5,5-tetramethyl-3-pyrrolin-1-yloxy (461 mg, 2.50 mmol) were dissolved in THF (12 mL). While cooling in an ice bath, (516 mg, 2.50 mmol) dicyclohexylcarbodiimide in THF (5 mL) tetrahydrofuran was added dropwise with a syringe. After 4 h the formed precipitate was separated by filtration and the yellow filtrate was washed with 2 mol L^{-1} HCl and brine, dried ($MgSO_4$), and concentrated. Column chromatography (SiO_2; dichloromethane/ethyl acetate 2 : 1) gave **3** (160 mg, 37%) as pale yellow crystals, mp. 250–253°C (dec.). FD-MS: $m/z = 516.8$ (100%, M^+).

The flexible oligomethylene biradical **4** was kindly supplied by Ciba-Geigy, Basel. For the DEER measurements, toluene solutions with a total biradical concentration of 1 mmol L^{-1} were filled into the EPR sample tubes, shock-frozen by immersion into liquid nitrogen, and transferred to the cooled probehead. For the biradical with an end-to-end distance of 5 nm, a concentration of 0.2 mmol L^{-1} was used.

DEER Measurements

Dipolar time evolution data were obtained at X-band frequencies with a Bruker Elexsys E 580 spectrometer using the four-pulse DEER experiment (*10, 11*). All biradical samples were measured at a temperature $T = 80$ K with a Bruker Flexline split-ring resonator ER 4118X-MS3, except for the sample of the longest biradical **2b** which was measured at $T = 15$ K with a Flexline pulse ENDOR resonator ER 4118X-MD5-EN. Both resonators were overcoupled to $Q \approx 100$. Pump pulses at a secondary microwave frequency were generated by feeding the output of an HP 83508 sweep oscillator to one microwave pulse forming unit of the spectrometer. The pump frequency was set to the maximum of the nitroxide spectrum, and the observer frequency was 60 MHz higher unless specified otherwise. Both the $\pi/2$ and π pulses had a length of 32 ns and the dwell time was 8 ns.

Comparison of Shell Factorization with Direct Conversion

For a critical test of distance resolution close to the lower limit of the distance range we selected a biphenyl-based biradical (for the structure, see inset in Fig. 5c). The background in the dipolar evolution data can be fit nicely by a second-order polynomial (Fig. 5a) with $t_1 = 320$ ns. The cross-talk-corrected Pake transform (Fig. 5b) exhibits a narrow peak at 1.92 nm, which is close to the expected spin–spin distance of 2 nm. An additional extremely narrow peak is observed at approximately 1.5 nm. This peak and its negative wings are an artifact due to

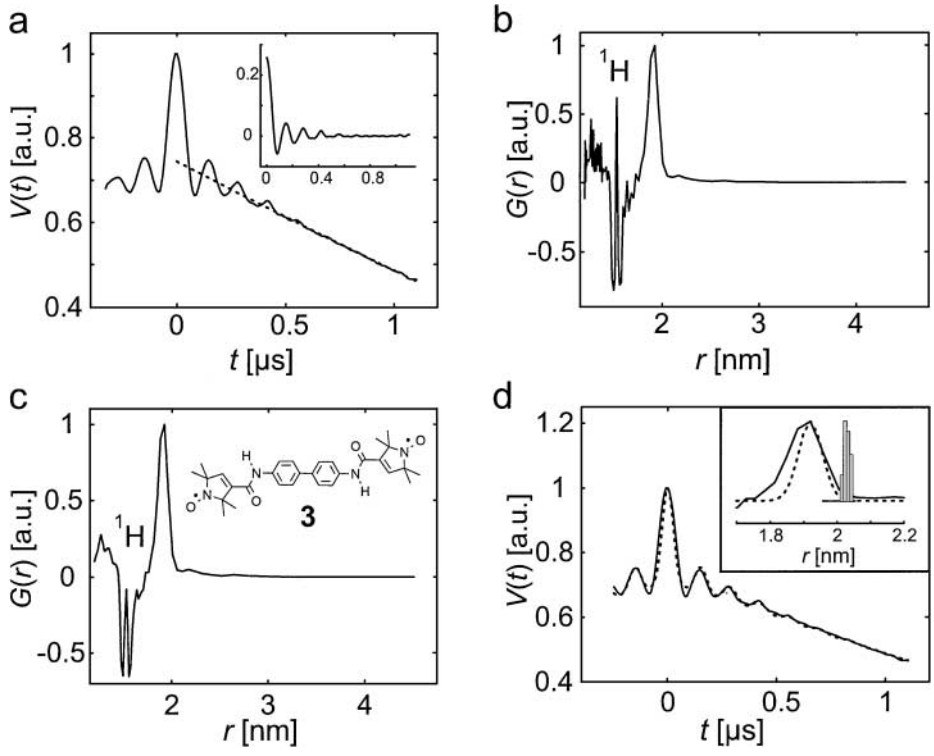

FIG. 5. Direct conversion of experimental dipolar time evolution data to a distance distribution for a shape-persistent biradical with a spin–spin distance of 1.92 nm. (a) Fitting of the nonlinear contribution. A second-order polynomial (dashed line) is fitted to the experimental data at $t \geq 320$ ns and subtracted. The inset shows the extracted linear contribution. (b) Distance distribution obtained by a cross-talk-corrected Pake transformation (no smoothing). The peak at approximately 1.5 nm is due to proton modulations. (c) Distance distribution obtained as in (b) but after convolution with a Gaussian function in the distance domain with a variance of 0.02 nm. (d) Experimental data (solid line) and fit by the shell factorization model (dashed line) assuming a distance distribution consisting of a single Gaussian peak at 1.92 nm with a variance of 0.05 nm and a homogeneous background with $\lambda c = 0.45$ mmol L^{-1}. The inset shows a comparison of the distance distribution obtained by direct extraction (solid line), in the shell factorization model (dashed line), and from a force-field conformer search (gray histogram).

^{1}H nuclear modulation. This artifact can be partially, but not completely, suppressed by adjusting the fixed interpulse delays τ_1 and τ_2 to a blind spot of the modulations (*10, 11*). If no such precautions are taken, as in our case, the distance distribution is significantly distorted for $r < 1.8$ nm. If DEER is performed at higher frequencies, the artifact is shifted toward shorter distances and ultimately out of the accessible distance range. For example, at Q-band frequencies ($\nu \approx 35$ GHz) the proton Zeeman frequency corresponds to a distance of 1.1 nm.

In this measurement, which took 14 h, the signal-to-noise ratio is sufficient to dispense with distance-domain smoothing. Nevertheless, convolution with a Gaussian function with a width of 0.02 nm improves the appearance of the distribution for low distances without broadening the peak at 1.92 nm (Fig. 5c). The dipolar evolution data can also be fit quite well using the shell factorization model and a distance distribution consisting of one Gaussian peak at 1.92 nm with a variance of 0.05 nm and a homogeneous background (Fig. 5d). The remaining deviations are due to orientation selection. As can be seen in the inset, there is a satisfying agreement between the distributions obtained by direct conversion (solid line) and modeling with a Gaussian peak (dashed line). A significant distortion of the distance distribution due to orientational selection effects is not apparent even for this system with low conformational freedom.

We have also compared the experimental distance distribution to the theoretical distance distribution in an ensemble of 48 conformers which was computed with the Merck Molecular Force Field using the Titan software package (Wavefunction Inc.). To avoid difficulties with the parametrization of nitroxide groups, these groups were substituted by keto groups. The electron spin was assumed to be localized at the center of the N–O bond. The distance between the centers of the two N–O bonds may be by approximately 0.07 nm shorter than the distance between the centers of the C=O groups in the diketone, as it was found for the conformer with the lowest energy by a BLYP density functional geometry optimization with the ADF (*39*) package (basis set IV, version 2000.02) as well as by a B3LYP density functional geometry optimization (basis set 6–31G*) with the Titan package. The theoretical distance distribution, corresponding to a Boltzmann distribution over the conformers at the melting point of toluene, is displayed as a histogram in the inset in Fig. 5d. This distribution is narrower than the experimental distribution and it is shifted by approximately 0.15 nm toward longer distances. This difference, which slightly exceeds the estimated combined

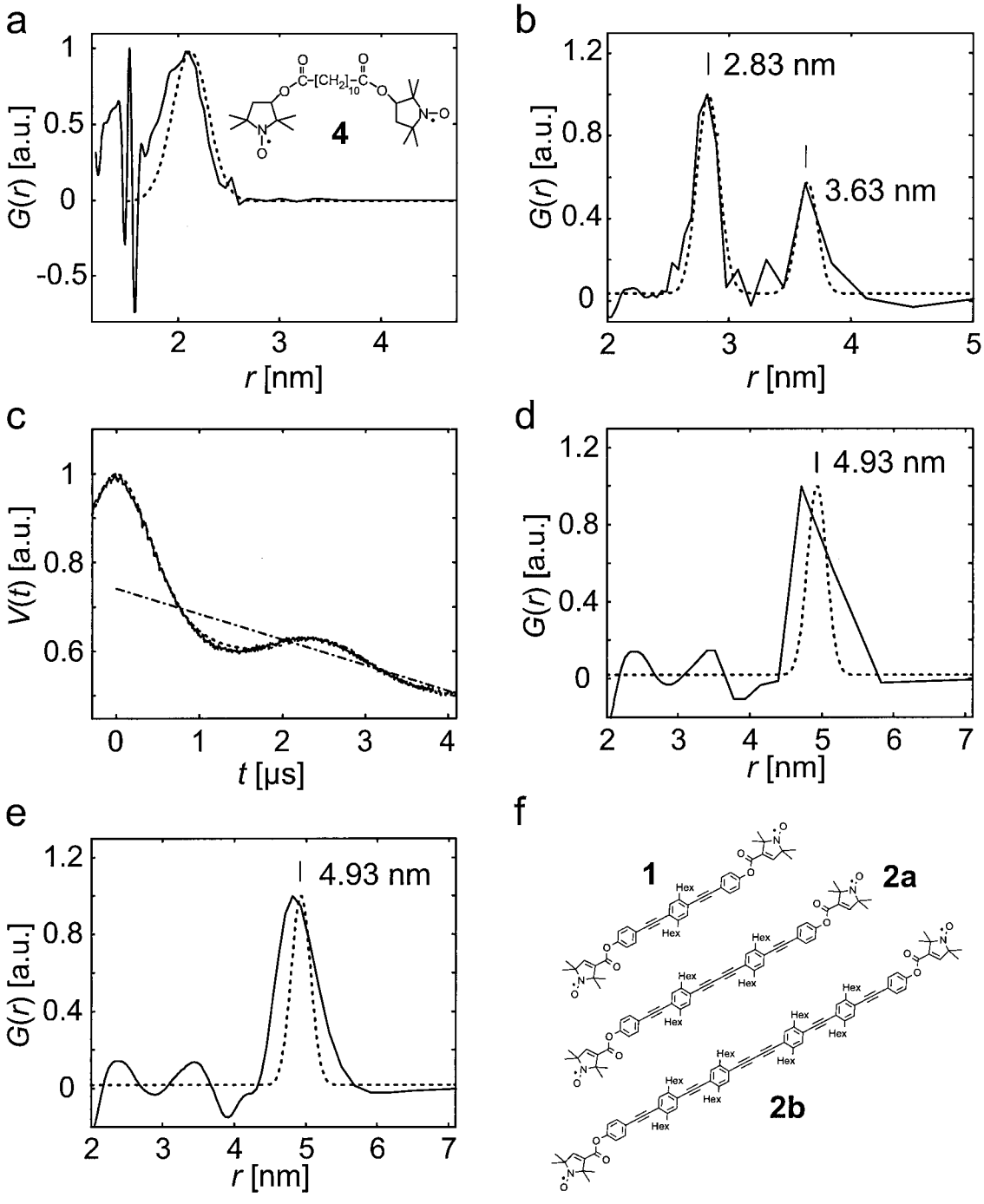

FIG. 6. Direct conversion of dipolar time evolution data to distance distributions for model compounds (solid lines) and fits with simple model distributions within the shell factorization model (dashed lines). (a) Flexible oligo (methylene) biradical with an average end-to-end distance of 2.1 nm. (b) Equimolar mixture ($c = 0.5$ mmol L^{-1} each) of two shape-persistent biradicals **1** and **2a** with distances of 2.83 and 3.63 nm (for structures, see Ref. *12*). (c) Dipolar evolution data of the shape-persistent biradical **2b** ($c = 0.2$ mmol L^{-1}) with an end-to-end distance of 4.93 nm. The dash-dot line is a linear background fit for $t \geq 1.2$ μs and the dashed line the best shell factorization fit obtained with a distribution consisting of a Gaussian peak ($r = 4.93$ nm, $\sigma = 0.19$ nm) and a homogeneous background. (d) Radial distribution function obtained by direct conversion of the data in (c) with Gaussian distance-domain smoothing ($\sigma = 0.2$ nm). (e) Radial distribution function obtained by zero-filling to 2048 points and direct conversion with Gaussian distance-domain smoothing ($\sigma = 0.1$ nm). (f) Structures of the shape-persistent biradicals **1**, **2a**, and **2b**.

uncertainties of the experiment and the force-field computation, might indicate a small exchange coupling between the two moieties of the molecule.

For a flexible oligomethylene biradical with 10 methylene units, the nonlinear background can again be fit nicely with $t_1 = 320$ ns and a second-order polynomial. After direct conversion, we obtain a much broader distance distribution with a maximum at 2.1 nm. Due to this broadening, distance-domain smoothing with a Gaussian function with a variance of 0.04 nm becomes necessary, although the measurement time was the same as for the biphenyl-based biradical. Furthermore, the artifact at 1.5 nm due to proton modulations becomes more prominent. Nevertheless, the distance distribution obtained by direct conversion (Fig. 6a) can be considered reliable for $r > 1.8$ nm. Again, the agreement between the distributions obtained by direct conversion (solid line) and modeling with a Gaussian peak using the shell factorization model (dashed line) is satisfying. Distortions due to orientational selection are not expected for this flexible biradical, as the orientations of the molecular frames of the two nitroxide groups are not strongly correlated. At least part of the deviation between the two curves is due to the fact that the end-to-end distance of these biradicals is not expected to exhibit a Gaussian distribution in a $G(r)$ plot (*40, 41*). The access to experimental distance distributions, rather than only mean distances, should allow for more detailed checks of theoretical models for chain conformation statistics.

To compare shell factorization and direct conversion at somewhat larger distances we used an equimolar mixture of the shape-persistent biradicals **1** and **2a** ($c_{\mathbf{1}} = c_{\mathbf{2a}} = 0.5$ mmol L^{-1}) with end-to-end distances of approximately 2.8 and 3.6 nm (for the structures, see Fig. 6f). Because of the slower decay of the linear contributions for the larger distances, we used $t_1 = 480$ ns for the background correction, which was again performed with a second-order polynomial. The results obtained by direct conversion and by a shell factorization fit with a distance distribution consisting of two Gaussian peaks and a homogeneous background agree well (Fig. 6b). The mean distances in the shell factorization fit ($r_{\mathbf{1}} = 2.83$ nm, $r_{\mathbf{2a}} = 3.64$ nm) also agree within 0.01 nm with our earlier fits of DEER data for these biradicals which neglected any effects of nonlinearity (*12*). However, the widths of the two peaks are now found to be approximately equal ($\sigma_{\mathbf{1}} = 0.13$ nm, $\sigma_{\mathbf{2a}} = 0.12$ nm), in contrast to the earlier fits. If we consider that $P(r) = 4\pi r^2 G(r)$ is the proper distribution function for a comparison of integral intensities, we find an experimental ratio of $c_{\mathbf{1}} : c_{\mathbf{2a}} = 1.18$, which is in satisfying agreement with the expected ratio of 1.0 given the error in weighing only a few milligramms of the substances. A distortion due to orientational selection might be expected as a ghost peak at 2.25 nm, corresponding to twice the dipolar frequency for the peak at 2.83 nm. No such peak is seen, which indicates again that orientation selection at X-band frequencies is too weak to be recognized with this kind of data analysis.

Finally we have tested the agreement between direct conversion and shell factorization for biradical **2b** of Ref. (*38*) (for the structure, see Fig. 6f). In this case the end-to-end distance of approximately 5 nm is close to r_{lin}, so that a precise elimination of the nonlinear contributions is more difficult and the resolution in $G(r)$ is severely limited. It is therefore crucial to work at low concentrations to have smaller nonlinear contributions and to measure the data in a longer time window. We found that a sufficient signal-to-noise ratio in a four-pulse DEER measurement could still be obtained in a measurement time of 16 h with a biradical concentration of 0.2 mmol L^{-1} and with $\tau_1 = 400$ ns and $\tau_2 = 5$ μs (Fig. 6c). For this low concentration and long distance, the background was best fitted by a linear function ($q = 1$) with $t_1 = 1.2$ μs (dash-dot line). The shell factorization fit (dashed line) again exhibits slight differences from the experimental data that can be traced back to orientation selection. The radial distribution function obtained by direct conversion and distance-domain smoothing with $\sigma = 0.2$ nm is in general agreement with the one obtained by a shell factorization fit. However, for this long distance the resolution is rather poor with direct conversion. Zero-filling of the experimental data to 2048 points before the integral transformation significantly improves resolution and agreement with the shell factorization fit without introducing significant distortions (Fig. 6e). Apodization of the data by a Hamming window before zero-filling causes significant broadening in the Pake transform (data not shown). Even with zero-filling, the agreement of peak width and peak maximum remains worse than for the shorter distances. The apparent line broadening with direct conversion may indicate a slightly incomplete separation of linear and nonlinear contributions. As predicted by theory, a distance of 5 nm may thus correspond to the upper limit for the direct conversion approach, unless even lower concentrations and longer time windows can be used.

CONCLUSION

In the limit of small modulation depths, angular correlations between spin pairs can be neglected and dipolar time evolution data can be analyzed in terms of a spin–spin distance distribution. For disordered systems, the dipolar time evolution data can be quantitatively simulated by integrating the signal over thin spherical shells and multiplying the signals of all the shells (shell factorization model). The contribution due to electron spin pairs with distances smaller than about 5 nm is closely approximated by integration over the distance distribution, as used in earlier work. To a good approximation, the nonlinear contribution due to spins at longer distances can be eliminated from the data by fitting a low-order polynomial to the data after a certain threshold time t_1, extrapolating this polynomial to time zero, subtracting it, and dividing the residual by the same polynomial. The extracted linear contribution to the data can be directly converted to a distribution of dipolar coupling frequencies by a cross-talk-corrected integral transformation and mapped to a distance distribution or to the radial distribution function $G(r)$. Excessive noise in $G(r)$ at short distances can be suppressed by

convolution with a Gaussian function of constant width in the distance domain. Experiments on shape-persistent and flexible biradicals with end-to-end distances between 2 and 5 nm confirm that radial distribution functions obtained by such a direct conversion are in satisfying agreement with radial distribution functions obtained by fits with the shell factorization model and with theoretical expectations. As the latter model considers nonlinear effects directly and quantitatively, this demonstrates that nonlinear effects can be neglected for $r \lesssim 5$ nm and that the contributions due to pairs with larger spin–spin distances are effectively eliminated by the procedure described above.

ACKNOWLEDGMENTS

The authors thank Christian Bauer for technical support and Dr. C. Kröhnke (Ciba-Geigy AG) for supplying the oligomethylene biradical. Detailed comments by an anonymous referee are gratefully acknowledged.

REFERENCES

1. L. J. Berliner, S. S. Eaton, and G. R. Eaton (Eds.), "Biological Magnetic Resonance," Vol. 19, Kluwer, New York (2001).
2. O. Kratky and O. Glatter (Eds.), "Smaller Angle X-ray Scattering," Academic Press, London (1982).
3. J. S. Higgins and H. C. Benoit, "Polymers and Neutron Scattering," Clarendon Press, Oxford (1994).
4. P. Wu and L. Brand, *Anal. Biochem.* **218,** 1–13 (1994).
5. A. Schweiger and G. Jeschke, "Principles of Electron Paramagnetic Resonance," Oxford University Press, Oxford (2001).
6. A. D. Milov, K. M. Salikhov, and M. D. Shirov, *Fiz. Tverd. Tela (Leningrad)* **23,** 957 (1981).
7. A. D. Milov, A. B. Ponomarev, and Yu. Tsvetkov, *Chem. Phys. Lett.* **110,** 67 (1984).
8. A. M. Raitsimring and K. M. Salikhov, *Bull. Magn. Reson.* **7,** 184 (1985).
9. A. D. Milov, A. G. Maryasov, and Yu. D. Tsvetkov, *Appl. Magn. Reson.* **15,** 107 (1998).
10. M. Pannier, S. Veit, A. Godt, G. Jeschke, and H. W. Spiess, *J. Magn. Reson.* **142,** 331–340 (2000).
11. G. Jeschke, M. Pannier, and H. W. Spiess, *in* "Biological Magnetic Resonance" (L. J. Berliner, S. S. Eaton, and G. R. Eaton, Eds.), Vol. 19, Chap. II, Kluwer, New York (2001).
12. G. Jeschke, M. Pannier, A. Godt, and H. W. Spiess, *Chem. Phys. Lett.* **331,** 243 (2000).
13. S. Saxena and J. H. Freed, *Chem. Phys. Lett.* **251,** 102 (1996).
14. S. Saxena and J. H. Freed, *J. Chem. Phys.* **107,** 1317 (1997).
15. P. Borbat and J. H. Freed, *Chem. Phys. Lett.* **313,** 145 (1999).
16. R. G. Larsen and D. J. Singel, *J. Chem. Phys.* **98,** 5134 (1993).
17. A. G. Maryasov, Yu. D. Tsvetkov, and J. Raap, *Appl. Magn. Reson.* **14,** 101 (1998).
18. M. Pannier, V. Schädler, M. Schöps, U. Wiesner, G. Jeschke, and H. W. Spiess, *Macromolecules* **33,** 7812 (2000).
19. M. Pannier, M. Schöps, V. Schädler, U. Wiesner, G. Jeschke, and H. W. Spiess, *Macromolecules* **34,** 5555 (2001).
20. A. M. Raitsimring and V. V. Tregub, *Chem. Phys.* **77,** 123 (1983).
21. V. V. Kurshev, A. M. Raitsimring, and T. Ichikawa, *J. Phys. Chem.* **95,** 3565 (1991).
22. A. D. Milov, A. G. Maryasov, Y. D. Tsvetkov, and J. Raap, *Chem. Phys. Lett.* **303,** 135 (1999).
23. A. Y. Pusep and N. V. Shokirev, *Opt. Spektrosk.* **57,** 792 (1984); Opt. *Spectrosc.* **57,** 482 (1984).
24. A. M. Raitsimring, L. A. Rapatskii, and N. V. Shokhirev, *Chem. Phys.* **105,** 117 (1986).
25. J. R. Klauder and P. W. Anderson, *Phys. Rev.* **125,** 912 (1962).
26. A. M. Raitsimring, K. M. Salikhov, B. A. Umanskii, and Yu. D. Tsvetkov, *Sov. Phys. Solid State* **16,** 492 (1974).
27. A. D. Milov and Yu. D. Tsvetkov, *Appl. Magn. Reson.* **18,** 217 (2000).
28. R. R. Ernst, G. Bodenhausen, and A. Wokaun, "Principles of Nuclear Magnetic Resonance in One and Two Dimensions," Clarendon, Oxford (1987).
29. M. Bloom, J. H. Davis, and A. L. MacKay, *Chem. Phys. Lett.* **80,** 198 (1981).
30. E. Sternin, M. Bloom, and A. L. MacKay, *J. Magn. Reson.* **55,** 274 (1983).
31. K. Whitall, E. Sternin, M. Bloom, and A. L. MacKay, *J. Magn. Reson.* **84,** 64 (1989).
32. M. A. McCabe and S. R. Wassall, *J. Magn. Reson. B* **106,** 80 (1995).
33. H. Schäfer, B. Mädler, and F. Volke, *J. Magn. Reson. A* **116,** 145 (1995).
34. K. T. Mueller, T. P. Jarvie, D. J. Aurentz, and B. W. Roberts, *Chem. Phys. Lett.* **242,** 535 (1995).
35. D. Lemoine, *J. Chem. Phys.* **101,** 3936 (1994).
36. J. L. Hoch and A. S. Stern, "NMR Data Processing," Wiley–Liss, New York (1996).
37. A. N. Tikhonov and V. Y. Arsenin, "Solutions of III-Posed Problems," Wiley, New York (1977).
38. A. Godt, C. Franzen, S. Veit, V. Enkelmann, M. Pannier, and G. Jeschke, *J. Org. Chem.* **65,** 7575 (2000).
39. C. Fonseca Guerra, J. G. Snijders, G. te Velde, and E. J. Baerends, *Theor. Chem. Acc.* **99,** 391 (1998).
40. V. Pfannebecker, H. Klos, M. Hubrich, T. Volkmer, A. Heuer, U. Wiesner, and H. W. Spiess, *J. Phys. Chem.* **100,** 13428 (1996).
41. P. J. Flory, "Statistical Mechanics of Chain Molecules," Wiley–Interscience, New York (1969).